This is a repository copy of *Three-dimensional static and dynamic analysis of a composite cruciform structure subjected to biaxial loading: a discontinuum approach*.

White Rose Research Online URL for this paper:
http://eprints.whiterose.ac.uk/90590/

Version: Accepted Version

Three-dimensional static and dynamic analysis of a composite cruciform structure subjected to biaxial loading: a discontinuum approach

J.Navarro-Zafra · J.L. Curiel-Sosa · M.C Serna Moreno

Abstract A three-dimensional structural integrity analysis using the eXtended Finite Element Method (XFEM) is considered for simulating the crack behaviour of a chopped fibre-glass-reinforced polyester (CGRP) cruciform specimen subjected to a quasi-static tensile biaxial loading. This is the first time this problem is accomplished for computing the stress intensity factors (SIFs) produced in the biaxially loaded area of the cruciform specimen. A static crack analysis for the calculation of the mixed-mode SIFs is carried out. SIFs are calculated for infinite plates under biaxial loading as well as for the CGRP cruciform specimens in order to review the possible edge effects. A ratio relating the side of the central zone of the cruciform and the crack length is proposed. Additionally, the initiation and evolution of a three-dimensional crack are successfully simulated. Specific challenges such as the 3D crack initiation, based on a principal stress criterion, and its front propagation, in perpendicular to the principal stress direction, are conveniently addressed. No initial crack location is pre-defined and an unique crack is developed. Finally, computational outputs are compared with theoretical and experimental results validating the analysis.

J. Navarro-Zafra
Department of Mechanical Engineering, The University of Sheffield, Sir Frederick Mappin Building, Mappin Street, S1 3JD Sheffield, United Kingdom
Tel.: +44 0014-22-7794
E-mail: jnavarrozafra1@sheffield.ac.uk

J.L Curiel-Sosa
Department of Mechanical Engineering, The University of Sheffield, Sir Frederick Mappin Building, Mappin Street, S1 3JD Sheffield, United Kingdom

M.C Serna Moreno
Escuela Técnica Superior de Ingenieros Industriales de Ciudad Real, Universidad de Castilla-La Mancha, Departamento de Mecánica Aplicada e Ingeniería de Proyectos, INEI Avenida Camilo José Cela s/n, 13071 Ciudad Real, Spain

1 Introduction

Advanced composite materials (ACM) are widely used in many industrial sectors such as aircraft industry, automobile industry, etc. Fundamentally, their interest is attributed to its properties: high strength-weight ratio, excellent resistant to fatigue and corrosion, satisfactory durability. However, because of the complex mechanical behaviour of these high-performance materials many experimental tests are required for designing safe components [6]. As an alternative for reducing the high number of experimental tests computational modelling is a remarkable approach.

Nowadays, by means of computer simulations, many phenomena of interest have already been successfully simulated e.g. car crash, a human aorta with an aneurysm, etc [15]. Nevertheless, other computational applications in the industry and the scientific community remain unsolved. In computational terms, a well-known numerical method is the Finite Element Method (FEM)[3]. Most of structural integrity analyses using FEM have been based in continuum damage mechanics, see for instance some works applied to composites in [10] [9] [5]. This paper is proposing a discontinuous approach as explained below. When using FEM for simulating moving cracks throughout a material, several limitations are observed [7]. To accurate represent discontinuities with FEM it becomes necessary to conform the discretization to the discontinuity. Then, in the case of crack propagation the mesh is re-generated at each crack-growth increment with a considerable computational cost.

Over the last decades several approaches for modelling material discontinuities have been proposed based on the partition of unity method [14], as the GFEM [11] or the XFEM [4] developed by Belytschko and Black in 1999. In particular, XFEM permits the representation of discontinuities independently of the mesh. This characteristic makes this method able to model moving cracks with no update of the mesh during crack propagation. New developments in analysis of crack growth modelling are carried out since XFEM came up [1], for instance the implementation of XFEM in 3D [22], the implementation of XFEM in $ABAQUS^{TM}$ [12], the delamination of GLARE [8], etc. For interested readers, a detail understanding of XFEM is presented in the work of Mohammadi [21].

In industrial applications using ACM, different complex loading cases are perceived. For instance, in the fuselage of an aircraft multi-axial loadings are observed during working conditions. Then, it is required a better understanding of these materials under multiple loading in different directions [20]. In this article a 3D CGRP composite specimen is studied submitted to in-plane biaxial loading. A static analysis for the calculation of the mixed-mode SIFs into infinite plates is carried out. The values of SIFs obtained by XFEM into the infinite plates are compared with the theoretical solution from literature. This analysis serves to validate the 3D XFEM capabilities for the calculation of SIFs into the composite considered. Once it is demonstrated that XFEM is able to accurately obtain the SIFs with a known case, SIFs are calculated for the cruciform specimens within the region where a biaxial loading is localized.

The calculation of SIFs into the cruciform specimen are influenced by the edge effects of the specimen. A ratio relating crack size and the dimensions of the cruciform is proposed. The proposed ratio allows edge effects to be minimized with the smallest cruciform design possible. In the best authors knowledge, the SIFs calculation into a CGRP cruciform submitted to biaxial loading by means of XFEM has never been undertaken. Additionally, a 3D moving crack initiation and propagation into the structure is simulated. The crack is developed as a natural outcome for all geometries based on the maximum stress criterion. Computational results are validated with experimental tests.

The studied cruciform is designed for reproducing a pure biaxial loading in its central zone where shear is negligible. The CGRP composite under study behaves in a quasi-isotropic manner. This fact is justified because of the random distribution of the fibres throughout the matrix [18],[19].

The article is organized as follows. In section 2, an introduction to XFEM is presented briefly. In section 3, the numerical model considered for representing the crack behaviour of the CGRP structure is described. Section 4.1 compares computational and experimental results for three different cruciform geometries analysed under different biaxial in-plane loading cases. In Section 4.2 a static analysis of the cruciforms is completed and mixed-mode SIFs are calculated for infinite plates and the cruciform specimens under consideration. Finally, in section 5, the conclusions of the work are explained, summarizing the main achievements as a result of the research process.

2 A discontinuous approach/model based on the eXtended Finite Element Method

The general idea of the XFEM is based on including discontinuous enrichment functions to the approximation of displacements. For a 3D case, a single crack is considered (see Figure 1). The point x^* defines the crack front as depicted in Figure 1. It is defined also n as the normal to the crack plane. Then, the Heaviside function $H(x)$ takes value $+1$ if $(x - x^*) \cdot \boldsymbol{n} \geq 0$ and -1 otherwise, i.e.

$$H(x) = \begin{cases} 1 & \text{if} & (x - x^*) \cdot \boldsymbol{n} \geq 0 \\ -1 & \text{otherwise} \end{cases} \qquad (1)$$

The isotropic near-tip asymptotic functions $\psi_j(r, \theta)$ are included in the displacement approximation in order to represent the asymptotic crack-tip field.

$$\boldsymbol{\Psi}(x) = [\sqrt{r}cos(\frac{\theta}{2}), \sqrt{r}sin(\frac{\theta}{2}), \sqrt{r}sin(\theta)sin(\frac{\theta}{2}), \sqrt{r}sin(\theta)cos(\frac{\theta}{2})] \qquad (2)$$

Thus, once the Heaviside and the near crack-tip enrichment functions are considered in the element approximation of displacements, $\boldsymbol{u}^{(e)}$ it is obtained:
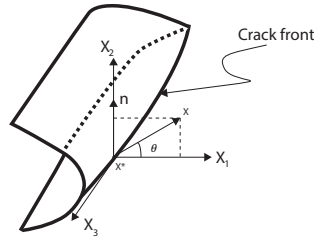
Fig. 1 Cordinate system for the crack front in 3D

$$\boldsymbol{u}^{(e)} = \sum_{i=1}^{nnodes} \boldsymbol{N}_i(x)(\boldsymbol{u}_i + \boldsymbol{H}(x)\boldsymbol{a}_i + \sum_{\alpha=1}^{4} \boldsymbol{\psi}_\alpha(x)\boldsymbol{b}_i^\alpha) \tag{3}$$

Where $\boldsymbol{N}_i(x)$ are the shape functions and **nnodes** the number of nodes per element. $\boldsymbol{u}_i$ corresponds with the nodal displacement vector used in FEM; $\boldsymbol{a}_i$ is the nodal enriched degree of freedom vector, $\boldsymbol{H}(x)$ is the Heaviside function, $\boldsymbol{b}_i^\alpha$ are nodal enriched degrees of freedom and $\boldsymbol{\psi}_\alpha(x)$ the elastic asymptotic crack-tip functions for representing the crack singularity. For the calculation of SIFs the software considers full enrichment in order to represent the displacement field ahead of the crack-tip. Instead, during 3D crack propagation analysis partial enrichment is considered. Particularly, the isotropic crack-tip enrichment functions are not taken into account and the only enrichment function is the Heaviside function $\boldsymbol{H}(x)$. Thus, during crack propagation the crack crosses at once a whole element without need of enriching nodes with crack-tip enrichment functions. Then, Eq.(3) becomes:

$$\boldsymbol{u} = \sum_{i=1}^{nnodes} \boldsymbol{N}_i(x)(\boldsymbol{u}_i + \boldsymbol{H}(x)\boldsymbol{a}_i) \tag{4}$$

In this work, SIFs are calculated for infinite plates and CGRP cruciforms. SIFs are extracted from the J-integral calculation [2]. This integral is a contour integral for bi-dimensional geometries and its definition in this application is extended to three-dimensional geometries. The relation between the J-integral J and SIFs for linear elastic material [13] is given by the following equation:

$$J = \frac{1}{8\pi}\boldsymbol{K}^T\boldsymbol{P}^{-1}\boldsymbol{K} \tag{5}$$

where $\boldsymbol{K} = [K_I, K_{II}, K_{III}]^T$ and $\boldsymbol{P}$ the pre-logarithmic energy factor tensor. Interested readers for a better understanding of fracture mechanics concepts can consult fracture mechanics references such as [2].

3 Numerical model

Three different cruciform geometries A, B and C (Figure 2) are studied. The ACM tested owns a polymer matrix with 20% volume of glass fibre reinforcement. This CGRP composite is considered as a quasi-isotropic due to the

uniformly random distribution of the fibres. The material properties are depicted in Table 1. In that table, E represents the modulus of elasticity, v the Poisson ratio, ϵ_{yeild} the yield strain and σ_{yield} the yield strength which are obtained in [19].
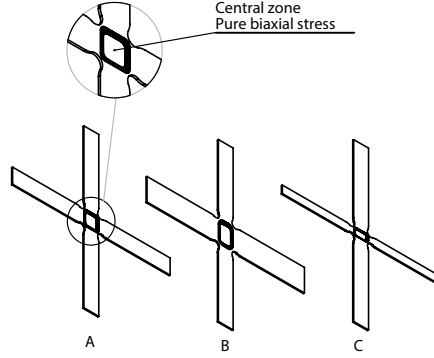

Fig. 2 CGRP cruciform specimens under analysis: geometry A, B and C. Notice a detailed view of geometry A in the central zone where pure biaxial loading state is observed.

Experimentally different biaxial loading cases are applied in each geometry. These loading cases cause failure through the diagonal of the central zone. 1/8 of the model for each geometry is simulated due to the symmetry. The boundary conditions applied to the three different geometries are depicted in Figure 3. Also, the cruciform specimen is fixed in the out-of-plane direction.

Fig. 3 Boundary conditions considered in the simulations for the three different cruciform geometries under biaxial loading: A,B and C.

For the finite element discretization, eight node hexahedral elements with reduced integration and three degrees of freedom per node are chosen (C3D8R). Reduced integration may provoke spurious zero-energy modes that provides an unreal solution. Therefore, hourglassing control is considered. A mesh convergence analysis is carried out for obtaining an adequate size mesh. Two different average size meshes are defined: 1.5 mm in the arms of the cruciform specimen and 0.5 mm in the central zone.

Table 1 Material parameters

$E(MPa)$	υ	$\sigma_{yield}(MPa)$	ϵ_{yield}	$G_I^C(N/m)$
6500	0.37	90	0.0138	6210

4 Computational and experimental crack behaviour of the CGRP cruciform specimen

In previous work, the authors presented a two-dimensional crack initiation and propagation analysis [17]. The computational results were validated by means of comparison with experimental results. In this paper, the main objective is focused in the calculation of SIFs for the real cruciforms submitted to biaxial loading as well as quantify the edge effects into each geometry. For making that possible, previous computational tests are needed. It is important to notice that in this work a 3D model is simulated. This model has not been validated before and higher numerical complexity is expected compare with the 2D case. Therefore, in Section 4.1 crack initiation and propagation is simulated within the 3D cruciform and compared with experimental outcomes. By means of this first computational analysis the three-dimensional abilities of XFEM are demonstrated. With the confidence of this analysis, the authors are able to go further when dealing with a 3D model. In Section 4.2, a 3D static crack analysis is carried out. This section can be divided into two main parts. The first part, Section 4.2.1, considers a quasi-infinite plate subjected to biaxial loading. Those plates are equivalent to the central zone of the cruciforms and SIFs are obtained using XFEM and afterwards compared with the theoretical solution. This analysis serves to show that XFEM is capable of accurately obtain SIFs in a biaxial loading context. The second part, Section 4.2, it is focused in the calculation of SIFs within cruciform specimens once the capabilities of XFEM has been validated in previous sections.

4.1 Crack initiation and propagation

4.1.1 Constitutive Model

The constitutive model for modelling crack initiation and propagation into the cruciform is defined by means of three characteristic steps (see Figure 4) and it needs to represent the fragile fracture process of the CGRP cruciform:
- Linear elastic traction-separation behaviour (point 1 to 2 in Figure 4). The elastic behaviour is defined in terms of elastic constitutive matrix that relates normal and shear stresses with nominal strains.
- Damage initiation (point 2 in Figure 4). It is connected with the beginning of the degradation of the cohesive response in an enriched element. The criterion of initiation selected is based on maximum principal stresses $\sigma_{max} = \sigma_{yield} \pm \sigma_{tol}$. Therefore, when the maximum principal stresses σ_{max}

achieve a value that it is the sum of yield stress σ_{yield} and a certain value of tolerance σ_{tol} (define by the user) the damage process starts.

- Damage evolution (point 2 to 3 in Figure 4). Once the initiation criterion is satisfied, damage evolution defines the degradation of the stiffness (softening). The constitutive relation is written as follows $\sigma = (1 - \omega)C\delta$, where ω is a scalar variable that is responsible for the degradation of the stiffness. Initially this variable is zero (full load-carrying capability) and at the end of the degradation process this variable takes value 1 (no load-carrying capability). For a proper definition of that variable, it is requested a critical fracture energy G^C for each pure failure mode. Based on experimental observations, the dominant mode of fracture in the cruciform specimen is mode I. Then, it is assumed that the mode I of failure defines the fracture process and consequently it is defined the critical energy for pure mode I of failure G_I^C. This energy G_I^C refers to the energy dissipated during the damage process per unit area and its value is estimated by means of uniaxial testing. Therefore, the energy dissipated per unit volume during damage evolution is $G_I^C = \frac{\sigma_{yield}0.01\epsilon_{yield}}{2}$ (Table 1). In this case, G_I^C is equal to the critical fracture energy per unit area because the traction-separation model considered a unitary cohesive thickness. Due to the brittle material behaviour of the composite, it is assumed that the fracture strain ϵ_u is 1% higher than the yield strain ϵ_{yield}.

Difficulties of convergence using implicit solver are detected when strain-
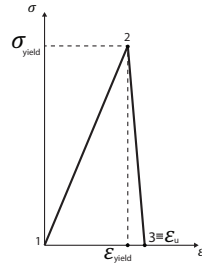

Fig. 4 Segment form by point 1 to 2: Undamaged liner elastic behaviour, point 2: damage initiation and segment form by point 2 to 3: softening.

softening behaviour is modelled. For solving this difficulty, a viscous regularization of the constitutive equations defining the cohesive behaviour is adopted. In the regularization scheme a viscous damage variable is defined $\omega_v = (\omega - \omega_v)/\eta$, where η is the viscosity coefficient that represent the relaxation of time of the viscous system and ω the damage variable in the inviscid model. The viscous coefficient η increments the rate of convergence of the model when it is dealing with strain-softening material behaviour. Then, using a small coefficient (small compared with a characteristic time t_c of the system) convergence can be improved. For this application, the characteristic time is calculated based on the stress wave velocity of propagation and its value is 2.1 μs. It is no-

Table 2 Simulation parameters

Figure	Geometry	Loading case	$\sigma_{tol}[Pa]$	$\eta[s]$	Initial crack
$Figure5(b)$	A	1/2	1	10^{-7}	No
$Figure5(a)$	A	1/1	1	10^{-7}	No
$Figure6(a)$	B	1.5/1	1	10^{-3}	No
$Figure7$	C	0.5/1	1	10^{-3}	No

ticed that one of the viscous coefficient considered during crack propagation is higher than the characteristic time of the system. However, the viscous energy involved during simulations is a 0.16 % of the total internal energy stored in the system, then, the viscous regularization does not compromise the solution and realistic results are consequently provided. It is noticed that during this research the damage tolerance σ_{tol} and viscous parameter η have a considerable influence on the progression of the crack and the convergence of the solution. It is assumed that the specimen is in elastic equilibrium during the loading process so quasi-static simulations are developed employing an implicit solver for solving the momentum equation. An automatic time stepping is chosen. Maximum and minimum values of the time step are 10^{-2} and 10^{-20} respectively. 10000 increments per time step are used.

4.1.2 Validation of the 3D model by comparison with experimental tests

Experiments showed two main outcomes: the first is that the correct failure within the cruciform is when the crack transverse the central region submitted to biaxial loading in geometries A, B and C [18] and the second one is that each geometry owns a certain biaxial loading case where a crack is localized in the central zone. Considering that, simulations were carried out and the simulation parameters to aim a crack path crossing the central zone are presented in Table 2. In the current work, non a-priori crack location is defined for all geometries, thus, the crack is initiated and propagated as a solution-dependent. Damage initiation is properly predicted by XFEM and all geometries initiated a crack at 90 MPa in the rounded zone. Geometry A is submitted to a loading case 1/1, which means that the same load is applied in both arms. As a result of this loading condition, simulation results show a crack throughout the central zone of the geometry (figure 5 (a)) and the crack-path followed is similar to the experimental case. In geometry A, when the loading case is different to 1/1 an incorrect failure is detected (failure in the arm with bigger load). This fact is also predicted by XFEM. In Figure 5 (b), geometry A is submitted to a loading case 1/2 (double load in the vertical arm). Thus, the crack is developed in the arm suffering a higher load which is in good agreement with experiments. In the case of geometry B, the in-plane biaxial loading case applied is 1.5/1. As the previous example for geometry A, no pre-definition of the crack location is necessary, so as a natural outcome crack is initiated and propagated throughout the central zone. In figure 6 (a), it is depicted a
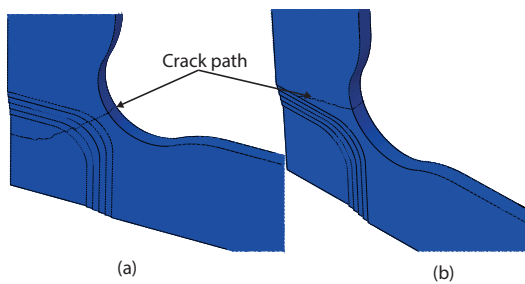
Fig. 5 (a) View of the crack propagation in geometry A under loading 1/1 without definition of a priori crack (b) View of the crack propagation in geometry A under loading 1/2 without definition of a priori crack

translucent view where the surface of the crack is appreciated in the 3D geometry. In Figure 6(b) it is illustrated the experimental results for geometry B under biaxial loading 1.5/1. That figure serves to illustrate the pattern of failure to achieve the correct collapse of the cruciform i.e. across the central zone. Geometry C is under a biaxial loading 0.5/1. Experimental results are accurately predicted by the simulations, therefore the computational crack is developed crossing the central zone (Figure 7).
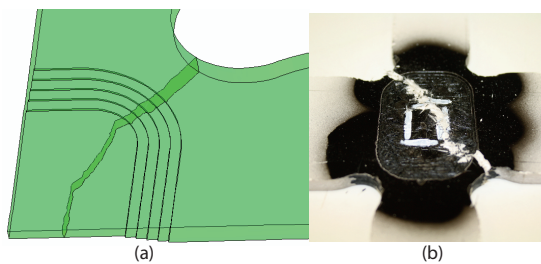

Fig. 6 (a) Computational crack propagation in geometry B under loading case 1.5/1 without definition of a priori crack location (b) Experimental path failure in geometry B for a biaxial loading 1.5/1 [18].
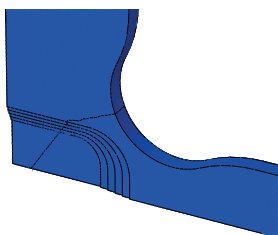

Fig. 7 Crack propagation in geometry C under loading 0.5/1 without definition of a priori crack.

4.2 Biaxial static crack analysis

In this section, a static crack analysis is carried out into the CGRP composite. Firstly, three different quasi-infinite plates are simulated with the objective of validating XFEM for the calculation of SIFs in a biaxial contest. The size of these quasi-infinite plates is proportional to the central zone of the cruciform specimens. Secondly, SIFs are also obtain for the real cruciforms and compared with the analytical solution for infinite plates. A 3D model is needed for studying static crack analysis [13] within the quasi-infinite plates and the cruciform specimens. The edge effects into the SIFs calculation are studied.

4.2.1 Inclined crack in a biaxial stress field

In this section, the objective is to validate XFEM for calculating the mixed-mode SIFs in a 3D biaxial scenario. Therefore, the part of the structure with interest is the central zone of geometry A,B and C because it is where a biaxial loading is located. To study independently these regions, rectangular plates are considered for simulations (see Figure 8). The dimensions of the plates (Table 3) are one order of magnitude higher that the original central zone on the cruciforms to consider the study of an ideal quasi-infinite plate respect to the real critical area. Thus, the solution of the SIFs in mode-I and mode-II is admissible and its expression is [16]:

$$K_I^{Theo} = \sigma\sqrt{\pi a}(sin^2\beta + \alpha cos^2\beta) \qquad (6)$$

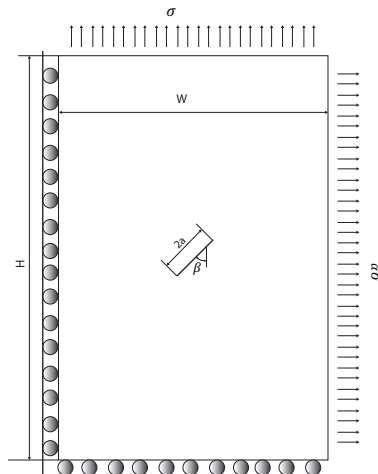$$K_{II}^{Theo} = \sigma\sqrt{\pi a}(1 - \alpha)cos\beta sin\beta \qquad (7)$$

where β is the angle form by the crack and the vertical direction, σ is the stress, a is half-crack length, K_I^{Theo} and K_{II}^{Theo} are the first and second theoretical mode SIF, respectively. α is defined as the ratio between the major and minor stress into the plate.

As it is illustrated in Figure 8, a centre crack is defined in each plate under analysis. This crack is 2 mm long for all geometries. The crack size chosen for this analysis is relatively small compared with the dimensions of the quasi-infinite plates considered. Therefore, the quasi-infinite plate can be considered as a infinite respect to the crack size and edge effects are then minimized. The crack under analysis is inclined with an angle β. This angle is the angle form between the crack and the vertical direction. This angle is subtracted from experiments and corresponds with the failure angle observed in the rounded zone for each geometry. The crack path is almost constant throughout the cruciform so the crack angle observed in the rounded zone is approximately the same as the central zone. Thus, for geometry A this angle is 45°, for B 33.69° and C 63.43°. The values of the load applied to the plates in each direction are depicted on Table 3. These values of stress correspond with the stress failure in the central region observed during experiments. Boundary conditions and loading directions in the plate are depicted in Figure 8. Note that plates are also constrained in the out-of-plane direction. In Figure 8, W

Table 3 Dimensions and loading in the infinite plates considered

Geometry	A	B	C
Dimensions plate(W|H)[mm]	220x220	220x330	220x110
Loading (σ_x-σ_y)[MPa]	84-84	81.8-49.9	48-103.5

represent the width and H the hight of the plates. Thus, different values of W and H are considered for simulations as shows Table 3.

Fig. 8 Boundary conditions of the centre crack under biaxial loading

In the neighbourhood of the crack location, it is considered a square area of 4x4 mm around a centre crack where 2500 elements are stacked in order to capture the crack-tip stress field. The major edges of the plate are partitioned into 80 equal subdivisions for each plate. The thickness of the plate is 2 mm and two mesh subdivision are considered throughout the thickness. SIFs obtain by simulations are presented in Table 3. The analytical solution is compared with the results obtained with XFEM.

Computationally, the J-integral is considered for the SIFs calculation. It is well-known that in theory the J-integral is path independent. However, computationally this is not true. Therefore, different contours give different solutions of SIFs. In this study five contours are taken into account. Because of numerical singularities, the first contour is not considered as it is suggested in [13]. Then, the SIFs depicted on Table 4 have been obtained as the mean of the five consecutive values starting from the second value of K_I and K_{II} calculated.

The theoretical values of SIFs are compared with the numerical ones obtained by means of XFEM. The small relative error appreciated between theoretical and numerical solutions confirms that XFEM is able to predict the

Table 4 SIFs for a 2 mm crack in the central zone of the plate

Geometry	β	K_I^{Theo}	K_{II}^{Theo}	K_I^{Num}	K_{II}^{Num}	$|error K_I|(\%)$	$|error K_{II}|(\%)$
A	45	4.70	0	4.56	0	3.06	0
B	33.69	3.34	0.82	3.36	0.85	5.68	3.01
C	63.43	5.17	1.24	5.13	1.29	0.9	3.74

mixed-mode fracture process here considered and validates its use for SIFs calculation considering a biaxial loading.

4.2.2 SIFs into the real cruciforms

In this section, SIFs are calculated for the real cruciform specimens and then compared with the theoretical solution. 1/8 of each cruciform is simulated with inclined cracks in the central zone. Different values of a i.e. half-size of the crack length, are considered, $a = 0.5, 1, 1.5, 2mm$. The angle of inclination β considered is the same as for the quasi-infinite plate analysed in previous section. Three different mesh regions can be distinguished with different element size in the structure. The first one defined is in the central zone with a 0.5 mm size, the second one defined in the arms with 1.5 mm size and the third one in the proximity of the static crack as depicted in Figure 9. For the third mesh refinement, a 4x4mm square is defined surrounding the crack with 1600 elements. The loading applied in this case is on the arms of the cruciform. Then, for geometry A, $54MPa$ are applied in each arm, in geometry B, $61MPa$ and in geometry C, $44.25MPa$. These values of load in each arm are responsible for the final fracture of the structure. The values of SIFs obtain with the quasi-infinite plates presented on Table 4 show that the values of K_I obtained by XFEM are higher than the ones K_II. This fact is also observed on Figure 10 for the cruciform structures. These results allow us to demonstrate numerically that the dominant mode of fracture is mode I. Comparing Table 4 and Figure 10 for $a = 1mm$ (2 mm of crack length), it is observed that the values of SIF calculated for quasi-infinite plates are closer than the SIF obtained for the cruciform specimen to the theoretical solution for an infinite plate. This fact it is explained because the quasi-infinite plates represent a similar configuration than the theoretical solution for an infinite plate. As mentioned previously, a pure biaxial loading is located on the central zone of the cruciform structure (see Figure 9). The magnitude of the horizontal and vertical stresses in this zone is the same as the ones applied in X and Y direction to the quasi-infinite plate depicted on Figure 8. Hence, in Figure 8 it is considered a quasi-infinite plate with loading conditions, angle of the crack and material properties identical as the central zone of the cruciform. Therefore, when considering these plates, the theoretical solutions for an infinite plate (Equations 6 and 7) provide SIF values close to values of SIF obtained numerically using XFEM (see Table 4). However, in the cruciform structure, when calculating SIF the theoretical solution for an infinite plate is not able to

provide results close to the ones computed numerically (see Figure 12 and 13). This is justified because the length of the area loaded biaxially is not infinite if it is compared with the size of the crack
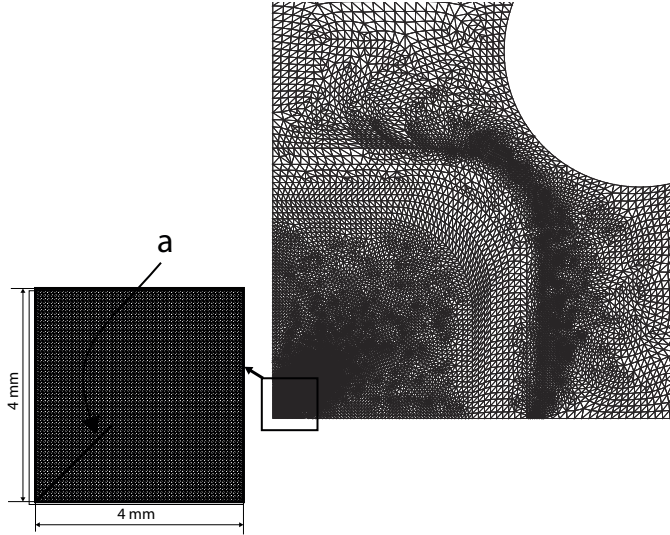

Fig. 9 Crack location in cruciform A for SIFs calculation. Note a 4x4 quadrilateral area where a special refinement is required to accurately represent the crack-tip behaviour.

In Figure 10 and 11 it is depicted the values of K_I and K_{II} obtained. These values calculated by means of XFEM are represented against the half-crack size considered for each cruciform. In theory, under a biaxial loading any increment of the crack length a (maintaining all other parameters constant) will always contribute to increment the values of SIFs. This tendency is observed numerically in Figure 10 and 11. However, it is noticed a reduction in the accuracy of the SIF calculation when the crack size is incremented within each geometry. This is due to the edge effects that influence the SIFs calculation when using XFEM. The influence of the edge effects for the SIFs calculation depends of the size of the central zone of each geometry as shows Figure 12 and 13. In these figures, the absolute value of the relative error between theoretical and numerical solution is presented. Higher values of error for K_I and K_{II} are found in geometry C while geometry B is noticed a less influence of the edge effects. This fact is explain because geometry B has bigger central zone than geometry C, then the edge effects are mitigated when considering a crack with the same length into both geometries. In other words, the central zone on geometry B is closer to the quasi-infinite plate than the central zone of geometry C. Considering the last outcome, a possible alternative to minimize the edge effects is to stablish a new ratio α between the crack size a and the dimensions of the central zone that will minimize the edge effects. In Equation 8 it is proposed a ratio considering a square central zone of side L and the

half-crack length a as follows:

$$\alpha = \frac{L}{a} = 66 \tag{8}$$

According to Equation 8, for a crack size bigger than $\frac{L}{66}$ not negligible edge effects into the SIF calculation are appreciated compared with the theoretical solution. Obviously, considering a specimen with a higher α edge effects are reduced. Additionally, this analysis serves to give us a first idea of the relation between central zone and the crack size and allow future experiment tests to by oriented according to the ratio presented. It is important to notice that the values of K_I are higher than K_{II} in the cruciform specimens. Therefore, taken into account the SIFs calculation with XFEM, for geometry A only mode I is observed and the shear does not exist. However, for geometry B and C it is noticed a mixed mode failure. The values of shear in geometries B and C are small compared with the normal stress. In previous studies, the shear has not been considered nevertheless here it is demonstrated computationally that it has its influence within geometry B and C.
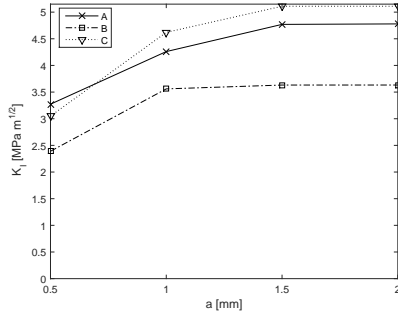

Fig. 10 K_I obtained by means of XFEM is represented against the half-crack length a defined for geometry A,B and C.

5 Conclusions

An investigation on the utility of the relatively novel numerical method XFEM applied to biaxial loading of composites has been presented. A static crack analysis is completed in order to determine the mixed-mode SIFs into CGRP cruciforms. Initially, SIFs are determined for infinite plates subjected to biaxial loading. Once the 3D XFEM model is validated, SIFs are also calculated for the whole cruciform specimens. By means of this analysis, it has been noticed that the edge effects into the cruciform specimens affects the SIFs values. The variation of SIFs values between the cruciform and the analytical solution are quantified. A ratio between the side of the central zone and the crack length is
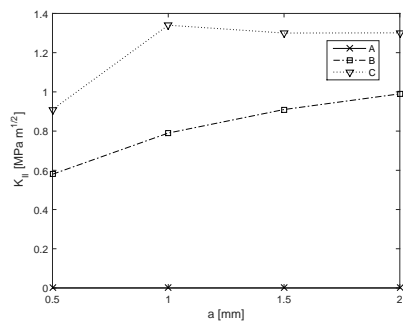
Fig. 11 K_{II} obtained by means of XFEM is represented against the half-crack length a defined for geometry A,B and C.
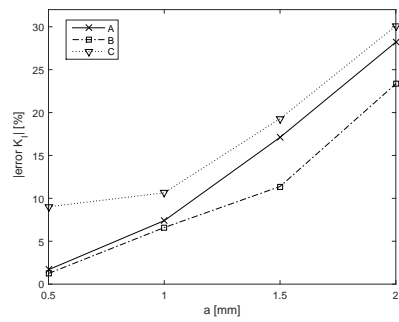

Fig. 12 The absolute relative error for mode-I $|error K_I|(\%)$ is represented against the half-crack length a for geometries A,B and C.
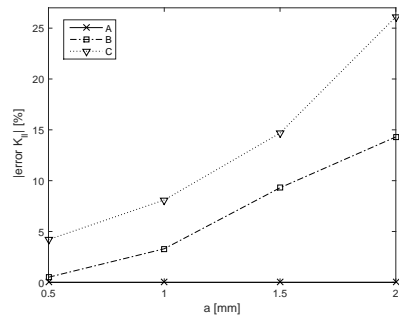

Fig. 13 The absolute relative error for mode-II $|error K_{II}|(\%)$ is represented against the half-crack length a for geometries A,B and C.

proposed in order to minimize edge effects and specimen size simultaneously. The dominant fracture mode into the cruciform structure is mode I according to the comparison between the numerical value of K_I and K_{II}. In other words, the nominal stress is higher than the shear stress during loading in the neigh-

bourhood of the crack tip. In the authors best knowledge, this is the first time that SIFs are calculated for this kind of CGRP cruciform specimens. Modelling initiation and propagation was not straightforward as has been shown above and challenges that are not an issue indeed becomes critical in a 3D context, overall when dealing with fracture. The following points were addressed during this research:

- Propagation of a 3D crack front without pre-notching.
- Criteria for crack initiation.
- Although re-meshing was not carried out, no deterioration of the solution was observed in terms of validation against experimental tests.

Overall, the application of XFEM here presented contributes to emphasizes that using XFEM for modelling crack in biaxial loading cases is adequate. Additionally, dealing with 3D XFEM a more realistic view of cracks is provided.

References

1. Abdelaziz, Y., Hamouine, A.: A survey of the extended finite element. Computers & Structures **86**(11), 1141–1151 (2008)
2. Anderson, T.L.: Fracture mechanics: fundamentals and applications. CRC press (2005)
3. Belytschko, T.: Nonlinear finite elements for continua and structures. Chichester : John Wiley, c2000, Chichester (2000)
4. Belytschko, T., Black, T.: ELASTIC CRACK GROWTH IN FINITE ELEMENTS **620**(July 1998), 601–620 (1999)
5. Carneiro Molina, A.J., Curiel-Sosa, J.L.: A multiscale finite element technique for non-linear multi-phase materials. Finite Elements in Analysis and Design **94**, 64–80 (2015)
6. Cox, B., Yang, Q.: In Quest of Virtual Tests for Structural Composites. Science **314**(5802), 1102–1107 (2006)
7. Curiel-Sosa, J.L., Brighenti, R., Serna Moreno, M.C., Barbieri, E.: Computational techniques for simulation of damage and failure on composites In Beaumont P, Soutis C & Hodzic A (Ed.). Structural Integrity and Durability of Advanced Composites Woodhead Publishing (2015)
8. Curiel-Sosa, J.L., Karapurath, N.: Delamination modelling of GLARE using the extended finite element method. Composites Science and Technology **72**(7), 788–791 (2012)
9. Curiel-Sosa, J.L., Petrinic, N., Wiegand, J.: A three-dimensional progressive damage model for fibre-composite materials. Mechanics Research Communications **35**(4), 219–221 (2008)
10. Curiel-Sosa, J.L., Phaneendra, S., Munoz, J.J.: Modelling of mixed damage on fibre reinforced composite laminates subjected to low velocity impact. International Journal of Damage Mechanics p. 1056789512446820 (2012)
11. Fries, T., Belytschko, T.: The extended/generalized finite element method: an overview of the method and its applications. International Journal for Numerical Methods in Engineering **84**(3), 253–304 (2010)
12. Giner, E., Sukumar, N., Tarancón, J., Fuenmayor, F.: An Abaqus implementation of the extended finite element method. Engineering Fracture Mechanics **76**(3), 347–368 (2009)
13. Hibbitt, Karlsson, Sorensen: ABAQUS/Standard user's manual, vol. 1. Hibbitt, Karlsson & Sorensen (2001)

14. Melenk, J.M., Babuška, I.: The partition of unity finite element method: basic theory and applications. Computer methods in applied mechanics and engineering **139**(1), 289–314 (1996)
15. Oden, J., Belytschko, T., Babuska, I., Hughes, T.: Research directions in computational mechanics. Computer Methods in Applied Mechanics and Engineering **192**(7-8), 913–922 (2003)
16. Rooke, D., Cartwright, D., of Defence, G.B.M.: Compendium of stress intensity factors. London: H.M.S.O. (1976)
17. Serna Moreno, M.C., Curiel-Sosa, J.L., Navarro-Zafra, J., Martínez Vicente, J.L., López Cela, J.J.: Crack propagation in a chopped glass-reinforced composite under biaxial testing by means of XFEM. Composite Structures (2014)
18. Serna Moreno, M.C., López Cela, J.J.: Failure envelope under biaxial tensile loading for chopped glass-reinforced polyester composites. Composites Science and Technology **72**(1), 91–96 (2011)
19. Serna Moreno, M.C., Martínez Vicente, J.L., López Cela, J.J.: Failure strain and stress fields of a chopped glass-reinforced polyester under biaxial loading. Composite Structures **103**, 27–33 (2013)
20. Soden, P.D., Hinton, M.J., Kaddour, A.S.: Biaxial test results for strength and deformation of a range of E-glass and carbon fibre reinforced composite laminates: failure exercise benchmark data. Composites Science and Technology **62**(12), 1489–1514 (2002)
21. (Soheil), S.M.: Extended finite element method for fracture analysis of structures. Oxford : Blackwell, c2008, Oxford (2008)
22. Sukumar, N., Moes, N., Moran, B., Belytschko, T.: Extended Finite element method for three-dimensional crack modelling (November 1999), 1549–1570 (2000)